Astron. Astrophys. 324, 1013–1019 (1997)

ASTRONOMY AND ASTROPHYSICS

Prompt entrainment in the variable molecular jet from RNO 15-FIR

Christopher J. Davis[1], **Jochen Eislöffel**[2,4], **Thomas P. Ray**[1], **and Tim Jenness**[3]

[1] School of Cosmic Physics, Dublin Institute for Advanced Studies, 5 Merrion Square, Dublin 2, Ireland
[2] Thüringer Landessternwarte, Karl-Schwarzschild-Observatorium, D-07778 Tautenburg, Germany
[3] Joint Astronomy Centre, 660 North A'ohōkū Place, University Park, Hilo, Hawaii 96720, USA
[4] Institute for Astronomy, University of Hawaii, 2680 Woodlawn Drive, Honolulu, HI 96822, USA

Received 24 December 1996 / Accepted 6 March 1997

Abstract. Optical, near-infrared, and sub-millimetre observations of the outflow from the young (Class I/Class 0) source RNO 15-FIR indicate that it is jet-driven, and that the "prompt" or bow shock entrainment mechanism dominates over "turbulent" entrainment. The CO J=3-2 observations presented in this paper reveal a collimated, bipolar, molecular outflow driven by RNO 15-FIR. The peaks in the CO outflow lobes are coincident with compact H_2 line emission features. We also find that the mass and momentum distributions in both flow lobes decrease with distance from the source, and that localised "peaks" in these distributions coincide with the H_2 knots. It is likely, therefore, that the H_2 knots represent bow shocks along the jet which accelerate ambient gas into the flow via a prompt entrainment mechanism.

Careful analysis of the data also suggests that the molecular outflow is "wiggling". This variation in flow direction is possibly due to the orbital motion of the outflow source about some unseen binary companion. The orbital period and binary separation estimated from a sinusoidal fit to the wiggling along the flow suggest two embedded sources with a combined mass of roughly $12M_{\odot}$.

Key words: ISM: clouds – ISM: jets and outflows – ISM: molecules – shock waves – infrared: ISM: lines and bands – infrared: stars

1. Introduction

There is growing support for the idea that massive molecular outflows from young stars are driven by collimated, high-velocity winds or "jets". The former are usually observed in maps of "moderate-velocity" molecular line emission, most often in CO J=1-0 or 2-1 (e.g. Bachiller 1996). The collimated jets, on the other hand, are traced by shocks which are observed at optical and/or near-infrared wavelengths; these shock features are well known as Herbig-Haro (HH) objects (Mundt, Brugel & Bührke 1987; Davis, Mundt & Eislöffel 1994; Ray 1996). However, we do not yet fully understand how the molecular outflows are driven by the jets.

Two general models prevail: (1) ambient, molecular gas may be swept up through bow shocks that develop at the head of, or along the length of, a collimated jet. This swept up gas cools rapidly and, although some of the gas may spill down the sides of the jet, a dense "clump" of gas collects just behind each bow shock. This scenario is referred to as the "prompt entrainment" model (De Young 1986; Masson & Chernin 1993; Raga & Cabrit 1993; Chernin et al. 1994). Alternatively, (2) ambient gas may be entrained along the length of the jet via a turbulent boundary layer (Stahler 1994; Taylor & Raga 1995; Raga, Cabrit & Cantó 1995). In this "steady-state" model, the turbulent layer will thicken with distance from the source, as more and more jet gas and ambient gas is pulled into the layer. Eventually, the jet itself will be completely pinched off and the flow will become fully turbulent.

In an effort to distinguish between entrainment models, Chernin & Masson (1995a) recently measured the distribution of momentum in a number of outflows. They point out that, in the turbulent entrainment model, the *momentum per unit length* should increase with distance from the source as more and more of the jet momentum (which we do not observe in CO) is transfered to the swept up molecular gas. Conversely, in the prompt entrainment model, the momentum decreases with distance from the source as the flow "accelerates" into the lower density regions further out (Masson & Chernin 1992). However, their results proved inconclusive in that the momentum profiles along the six outflows considered peaked roughly in the centre of each flow lobe.

Motivated by these ideas, however, and unswayed by this disappointing result, we have since obtained a fully-sampled CO J=3-2 map of the outflow driven by RNO 15-FIR (distance $\sim$ 350 pc; Herbig & Jones 1983). This outflow was discovered by Frerking & Langer (1982) and later mapped by Goldsmith

Send offprint requests to: C.J. Davis

et al. (1984) and Levreault (1988), although these maps had insufficient resolution to separate the outflow from other neighbouring systems. Hodapp (1994) and Davis et al. (1997) have more recently imaged the region at K′ and in H_2 respectively. Davis et al. discovered a sequence of compact H_2 line emission features which imply the presence of a highly-collimated, bipolar outflow. In this paper we present new optical and CO J=3-2 data. These allow us to distinguish between the various outflows in the region. We also attempt to distinguish between entrainment models for the RNO 15-FIR outflow, by (1) comparing the submillimetre data with the near-IR observations and (2) measuring the distribution of momentum along the flow lobes. We also search for evidence of flow variability in this system.

2. Observations

Optical observations of the RNO 15 and RNO 15-FIR region were obtained in October 1996 at the University of Hawaii 2.2 m telescope on Mauna Kea, Hawaii. The camera used employs a 2048×2048 pixel CCD with 24 μm pixels and a pixel scale of 0.″22. Images were obtained through a [S II] $\lambda\lambda$6716,6731 filter (λ_c = 6729Å, $\Delta\lambda$ = 28Å) and an I-band filter. Integration times were 1800 sec and 300 sec respectively.

The submillimetre data were taken at the James Clerk Maxwell telescope (JCMT) in July 1996. The telescope beam size at 345 GHz is 14″; the main-beam efficiency, $\eta_{\rm mb}$, is 0.58. A 55×15 point grid of CO 3-2 spectra, centred on RNO-15 FIR (R.A.(1950)= $03^{\rm h}\ 24^{\rm m}\ 34\overset{\rm s}{.}9$, Dec(1950)= 30° 02′ 40″) were observed, using the single channel SIS receiver B3i (Cunningham et al 1992) and the digital autocorrelation spectrometer (DAS) backend with a bandwidth of 250 MHz. The pointing accuracy of JCMT was checked regularly against Uranus and Saturn, and is better than 1.″5. The data were binned over two channels to a spectral resolution of 0.33 km/s. To map the outflow we employed a "raster scanning" technique. In this mode the spectrometer integrates while the telescope sweeps continuously along each row, a spectrum being "read-out" every 5″. An OFF position is observed at the end of each row; this is then subtracted from each ON spectrum. The spacing between each row was 5″, so the grid spacing in the final map is also 5″. The major axis of the grid was orientated along the outflow axis as defined by the H_2 knots (Davis et al. 1997); the position angle of this axis is 42°(E of N). The data were reduced using the SPECX package (although only linear baselines were removed from each spectrum). A single ^{13}CO spectrum was also observed towards the central map position (i.e. towards RNO 15-FIR).

3. Results

3.1. Optical outflows

In Fig. 1 we show a [SII] $\lambda\lambda$6716,6731 image of the RNO 15 and RNO 15-FIR region. In addition to knots B and C, which were discovered at near-IR wavelengths (Hodapp 1994; Davis et al. 1997), in [SII] there is another compact feature along the same outflow axis, though further away from RNO 15-FIR.

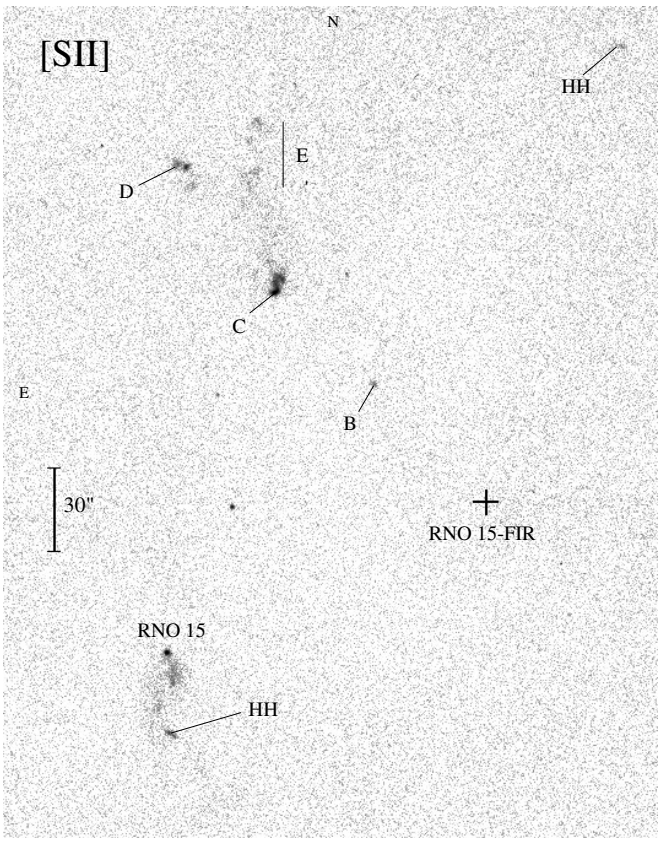

Fig. 1. [SII] $\lambda\lambda$6716,6731 image of the region around RNO 15 and RNO 15-FIR. The HH objects associated with the northeast-southwest outflow from RNO 15-FIR are labelled B-E. Additional line-emission features are marked 'HH'.

We label this feature knot D. We also observe a curious wisp of line-emission extending northward from knot C, which we label knot E; this feature does not appear to be part of the RNO 15-FIR outflow. Non of these features are evident in our I-band image (not shown here), so we regard them all as bona-fide HH objects. Knot C exhibits the same 'S'-shaped morphology in H_2 and [SII] (Davis et al. 1997; see also Fig. 4 below), the near-IR and optical emission being coincident. Knots D and E, on the other hand, are not observed in H_2, while the brightest H_2 knot, A, is not detected in [SII] (see Fig. 4 below). This all points to an increase in extinction, or molecular fraction in the local protostellar environment, towards the southwest (notably, the CS J=1-0 map of Juan et al. (1993) suggests such a trend). Indeed, since knot D and feature E are about 2.′5 ($\sim$ 0.25 pc) away from RNO 15-FIR, and because dense cores have typical diameters of about 0.15 – 0.35 pc (Myers et al. 1991), then it seems reasonable that somewhere just beyond knot C the outflow breaks out of the protostellar core that harbours RNO 15-FIR.

We have also labelled (with "HH" in Fig. 1) two other line emission features which are not observed in our I-band image. Neither appears to be associated with the RNO 15-FIR outflow, although both features may be part of the northwest-southeast

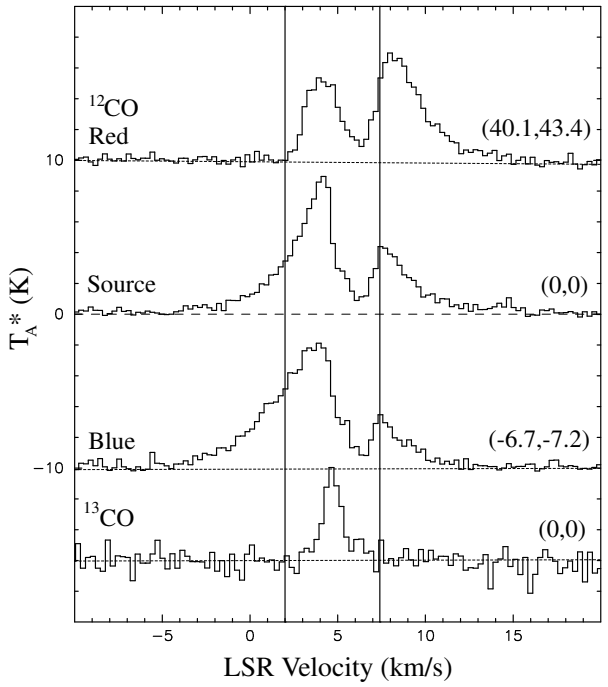

Fig. 2. ^{12}CO 3-2 spectra observed towards RNO 15-FIR (the (0,0) position in the map) and at peaks in the blue- and red-shifted outflow lobes (offsets in arcseconds are given at right). Also shown is a ^{13}CO 3-2 spectrum observed towards the source; this spectrum has been binned (over two channels) and multiplied by a factor of 2 for clarity. The vertical lines illustrate the velocities above and below which the red- and blue-shifted high-velocity gas is integrated in Fig. 4.

CO outflow driven by RNO 15 (Levreault 1988; see also Fig. 4 below).

3.2. CO outflows

In Figs. 2 to 4 we present the CO data, in the form of (1) representative spectra taken from the map, (2) a position-velocity (PV) diagram that is aligned with the outflow axis, and (3) an integrated-intensity map showing the blue- and red-shifted outflow lobes; this map is superimposed onto a near-IR image of the region (from Davis et al. 1997). A gaussian fit to the ^{13}CO spectrum observed towards RNO 15-FIR yields a mean LSR velocity of 4.7 km s^{-1}; this we identify with the systemic velocity, and consequently the integration limits in the outflow map are set longward and shortward of 7.4 km s^{-1} and 2.0 km s^{-1} respectively.

In the RNO 15-FIR outflow, the most pronounced blue-shifted wings are observed very close to the source (Fig. 2 & 3). Progressively weaker blue wings are observed with distance from the source. The red-shifted line wings (in the northeastern flow lobe) exhibit a similar, though less well defined, decrease in strength with distance from the source. We note, however, that there may be some confusion between the red-shifted lobe from RNO 15-FIR and the red lobe associated with RNO 15; the

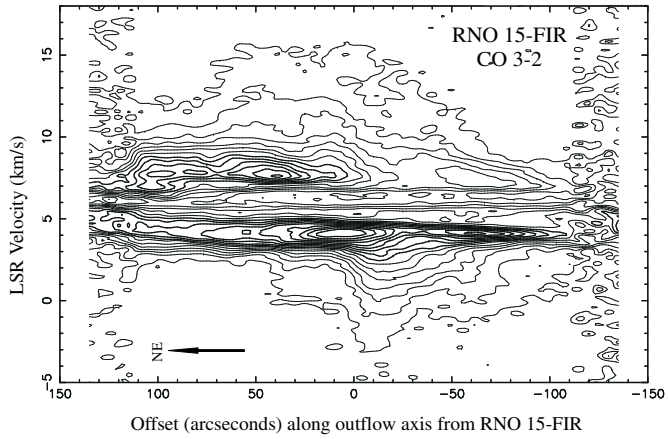

Fig. 3. Position-Velocity diagram along the outflow axis, constructed from the sum of the 9 strips of spectra observed between +20″ and -20″ of the flow axis.

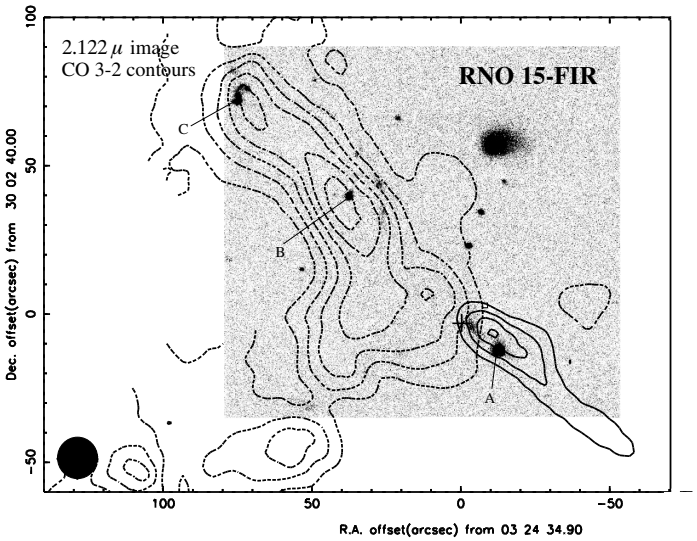

Fig. 4. A 2.122 μm image of the RNO 15-FIR outflow region (from Davis et al. 1997) with, overlayed, contours of the CO 3-2 integrated intensity. The integration interval in the blue-shifted flow lobe (full lines) is -5.0 to 2.0 km s^{-1}; the interval in the red-shifted lobe (dashed lines) is 7.4 to 14.4 km s^{-1}. The contours in both lobes increase in steps of 2 K km s^{-1} from a base contour level of 5 K km s^{-1}. The JCMT half-power beam size is indicated bottom-left. The cross marks the IRAS position of RNO 15-FIR; RNO 15 is offset by (108″,-58″) from RNO 15-FIR.

outflow from RNO 15 extends in roughly a northwest-southeast direction (Goldsmith et al. 1984; Levreault 1988).

In Fig. 4 the high-velocity CO map is superimposed onto the H_2 + continuum image of Davis et al (1997). The bipolar CO outflow lobes associated with RNO 15-FIR are clearly evident in this figure. Note, however, the red-shifted lobe of the outflow from RNO 15, which encroaches on the red lobe of the RNO 15-FIR outflow from the south-east.

The H_2 shocks, labelled A to C in Fig. 4, appear to be coincident with the peaks (or clumps) in the RNO 15-FIR CO outflow

map. This association has been observed in a number of other outflows (e.g. Bally et al. 1993; Davis & Eislöffel 1995; Dent, Matthews & Walther 1995; Davis et al. 1997). In all of these flows, there may well be a causal relationship between the H_2 shocks and CO clumps (discussed further below).

3.3. Parameters for the RNO 15-FIR CO outflow

We have calculated the mass ($\int T_b.dv$), momentum ($\int T_b.v.dv$) and energy ($\int T_b.v^2.dv$) in the blue- and red-shifted outflow lobes (Table 1). Note that the main beam brightness temperature used in these calculations is related to the antenna temperature, $T_{\rm A}^*$, by $T_b = T_{\rm A}^*/\eta_{\rm mb}$, where $\eta_{\rm mb}$ is the main-beam efficiency (Kutner & Ulich 1981). We assume optically thin emission in the line wings and gas in LTE. We use a $^{12}CO/H_2$ abundance ratio of 5×10^{-5}. Fukui et al. (1993) suggest that typical outflow temperatures range from 10 to 90 K; we therefore adopt an excitation temperature of 50 K, although the CO column density, derived from the J=3-2 line, is relatively insensitive to $T_{\rm ex}$ over this temperature range (to within a factor of 2).

The outflow masses quoted in Table 1 will be underestimated, because some of the low-velocity gas in the outflow will be "hidden" behind the ambient line profile. In a number of other outflows, the high-velocity mass fraction obeys a power law distribution of the form $m(v) \propto v^{-1.8}$ (Masson & Chernin 1992, 1993). If we assume this to be the case in the RNO 15-FIR outflow, then the mass fraction in the low velocity intervals 2.0 – 3.7 km s^{-1} and 5.7 – 7.4 km s^{-1} (excluded from our integration limits) could be as much as $\sim 3\times$ that traveling at higher velocities. However, the power law profile flattens out at low velocities (Lada & Fich 1996; Chandler et al. 1996), so the low-velocity mass fraction in RNO 15-FIR is probably much lower than this. Indeed, Cabrit & Bertout (1990) suggest that the mass of low-velocity gas hidden by the ambient cloud profile is typically twice that observed in the line wings.

The radial momentum, on the other hand, is a far better determined quantity, since the largest contribution comes from the higher-velocity line wings which are optically thin.

In Table 1 we also give estimates for the kinematic age and mechanical power in each flow lobe. The kinematic age is calculated from the mean velocity, $< V >$, which is weighted by mass (i.e. the ratio of the momentum to mass), and the length of each flow lobe, $R_{\rm max}$. Since $< V >$ is based on velocities measured along the line of site, and $R_{\rm max}$ is projected onto the plane of the sky, the kinematic age is a rather uncertain quantity. In fact, the momentum, energy and mechanical power are all affected by the unknown flow inclination angle. However, the partially overlapping flow lobes in RNO 15-FIR (Fig. 4) indicate that the outflow may be orientated at an angle of $\theta \sim 45°$, where θ is the angle between the outflow axis and the line of sight (Cabrit 1989). If this is the case, then the kinematic age (which has a correction factor of $\tan^{-1}\theta$) will be correct, while the momentum, energy and power (which have correction factors of $\cos^{-1}\theta$, $\cos^{-2}\theta$, and $\sin\theta\cos^{-3}\theta$), will only be underestimated by factors of 1.4, 2.0 and 2.0 respectively. We point out, however, that the kinematic age, when calculated in the manner described above, could be an overestimate of the "true age" of the system, since in a jet-driven outflow (discussed below), the jet (and bow shocks) will probably travel much faster than the swept-up CO gas. We also note, however, that the "ages" given in Table. 1 are marginally *lower* than the statistically implied outflow durations of Parker, Padman & Scott (1991).

The flow parameters listed in Table 1 describe a relatively weak molecular outflow when compared to other outflows from heavily embedded, young sources (e.g. Cep E – Ladd & Hodapp 1996; VLA 1623 – Dent et al. 1995; B335 – Moriarty-Schieven & Snell 1989). However, the values measured here for RNO 15-FIR exceed those recently measured for the outflow from, e.g. the more evolved HH 34 source (Chernin & Masson 1995b). Based on the correlation identified by Bontemps et al. (1996), between outflow power and both the source bolometric luminosity and circumstellar envelope mass, RNO 15-FIR may be a border-line Class 0/Class I source.

4. Discussion

4.1. Jet-driven molecular outflows: prompt or turbulent entrainment?

The high degree of collimation apparent in the RNO 15-FIR CO outflow, and the close association between the CO outflow and the Herbig-Haro Objects (knots A to C), implies that the outflow is driven by a collimated jet. The spatial coincidence between the 3 peaks in the CO integrated intensity map and the 3 molecular shocks traced in H_2 (Fig. 4) suggests that (1) these H_2 shocks are those which entrain much of the ambient gas to form the CO outflow, and that (2) the prompt entrainment mechanism dominates over turbulent entrainment.

In Fig. 5 we plot the mass per unit length (dM/dR), momentum per unit length (dP/dR), and mean velocity ($< V(R) >= [dP/dR]/[dM/dR]$) along the outflow axis, integrated across the width of the flow and over the high-velocity blue-shifted and red-shifted line wings. In both the northeastern, red-shifted flow lobe, and the southwestern, blue-shifted flow lobe, the mass and momentum decrease with distance from the source. This decrease is most dramatic in the blue-shifted lobe (at negative offsets in Fig. 5). Note also the localised "peaks" in dP/dR and dM/dR which coincide with the three H_2 knots A, B and C. The mean velocity, on the other hand, appears to be relatively constant along both flow lobes. This may be a direct consequence of the wing profiles being a power law in velocity ($m(v) \propto v^\gamma$; e.g. Masson & Chernin 1992) with the same index γ along the flow lobes.

Opacity at low outflow velocities is likely to have the most severe effect on the mass and (to a lesser extent) momentum estimates in Fig. 5. However, like Chernin & Masson (1995a) we find that these errors have little influence on the *distribution* of mass and momentum, since the mass and momentum profiles have the same overall shape (i.e. $< V(R) >$ remains virtually constant along the flow lobes) in spite of the fact that the momentum is weighted to higher velocities. Consequently,

Table 1. Mass, momentum and kinetic energy estimates (uncorrected for inclination angle). The velocity intervals used in the blue and red lobes are -5.0 – 2.0 km s^{-1} and 7.4 – 14.4 km s^{-1} respectively.

	Mass ($M_\odot$)	Momentum ($M_\odot$km s^{-1})	Energy ($\times 10^{35}$ J)	Kinematic Age ($\times 10^4$ yrs)	Mechanical Power ($\times 10^{-3}$ $L_\odot$)
Red Lobe	0.024	0.113	11.6	3.8	2.5
Blue Lobe	0.0026	0.011	1.03	2.4	0.35

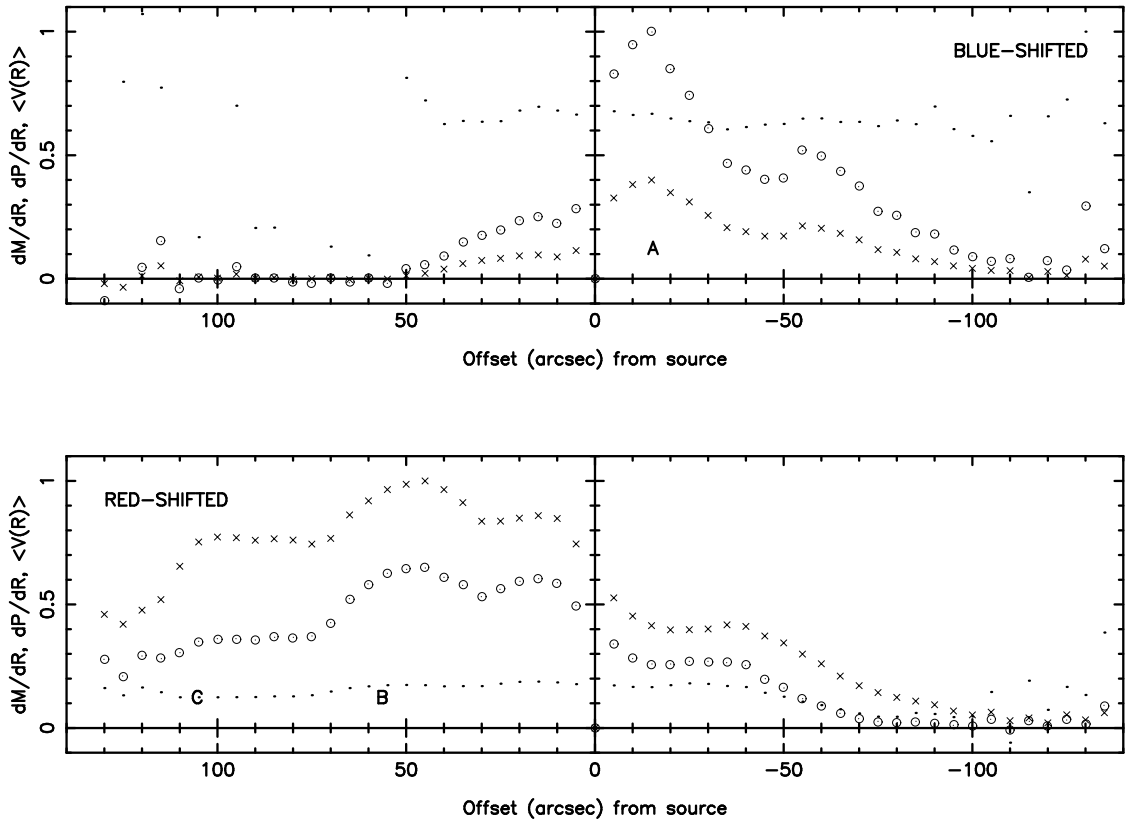

Fig. 5. Distribution of mass ($\int T_b.dv$ – crosses), momentum ($\int T_b.v.dv$ – dots+circles), and mean velocity (dots) along the RNO 15-FIR outflow axis, derived from the PV diagram in Fig. 3. Profiles for the blue-shifted ($v < 2.0$ km s^{-1}) and red-shifted ($v > 7.4$ km s^{-1}) high-velocity gas are plotted, measured at 5″ intervals, from the sum of 9 spectra in strips perpendicular to, though centred on, the outflow axis. dM/dR, dP/dR and $< V(R) >$ are normalised to the maximum measured values (scaling factors for dM/dR and dP/dR are 2.46×10^{14} [kg m^{-1}] and 7.15×10^{17} [kg s^{-1}] respectively). The offsets are in arcseconds from RNO 15-FIR (positive 'x' is towards the northeast). Labels A, B and C indicate the positions of the H_2 knots along the outflow axis.

the profiles in Fig. 5 are believed to be an accurate representation of the true distributions.

The decreasing momentum profiles, together with the coincidence of the H_2 knots and peaks in the dP/dR and dM/dR profiles, in both the blue-shifted and red-shifted flow lobes, therefore add considerable weight to the idea that *the prompt entrainment mechanism dominates in the RNO 15-FIR system*, and that the H_2 knots A, B and C represent bow shocks which entrain molecular gas into the flow.

In the prompt entrainment model, dP/dR is believed to be dependent on the distribution of ambient gas density (Masson & Chernin 1993), which probably follows a power law distribution of the form $\rho_o \propto R^{-1} \rightarrow R^{-2}$ (Shu, Adams & Lizano 1987). In Fig. 6 we therefore plot $log(dP/dR)$ against $log(R)$ for both blue- and red-shifted outflow lobes. A single straight-line fit does not seem appropriate in Fig. 6a (i.e. in the blue outflow lobe); instead, we fit two lines, one to the data measured within 50″ of the source ($log(R) < 1.7$), and a second to the data measured beyond this point. If we assume a power-law relationship

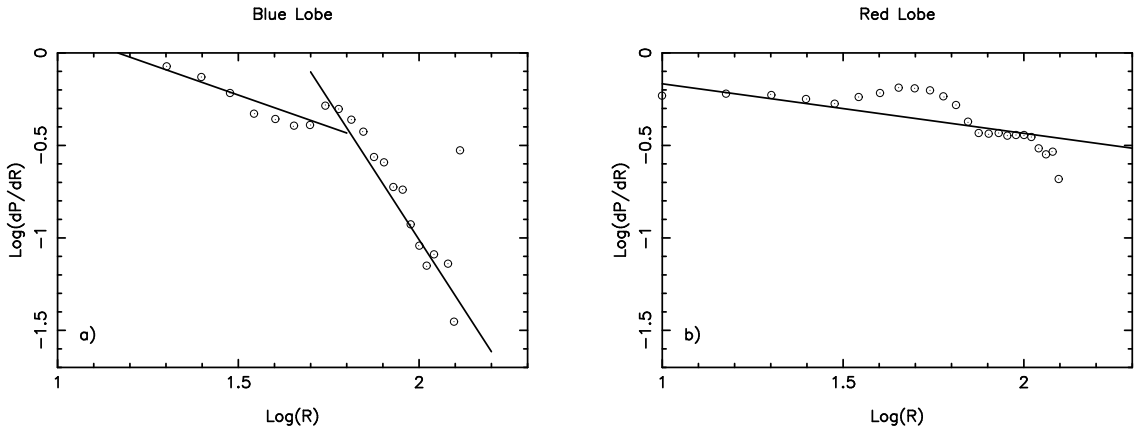

Fig. 6a and b. Least squares fits to the distribution of momentum per unit length (dP/dR) in the blue-shifted and red-shifted outflow lobes. dP/dR is normalised to the maximum measured value; R is in arcseconds.

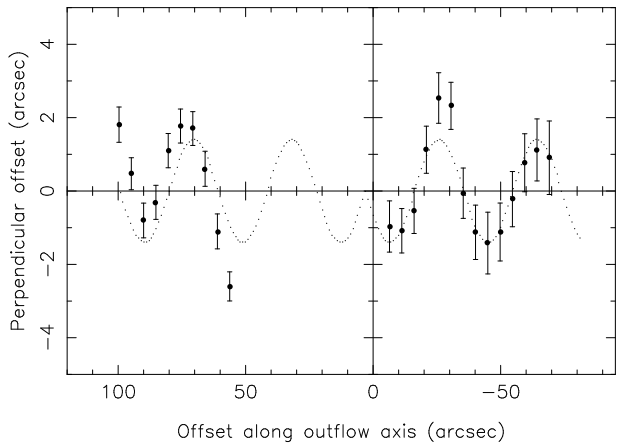

Fig. 7. Plot of high-velocity emission centroids (thick dots) along the outflow axis. Superimposed is a sinusoidal least-squares fit to the data. 3-σ error bars are also plotted.

of the form $dP/dR \propto R^{-\beta}$, then in the blue-shifted flow lobe β = 0.68 near to the source, while further out β = 3.02. In the red flow lobe, a single fit yields a value of β = 0.27 (Fig. 6b). If dP/dR is indeed dependent on the ambient gas distribution, then the sharp increase in β at $R \sim -50''$ (i.e. 0.085 pc) in the blue flow lobe may well be due to the outflow exiting the RNO 15-FIR protostellar core at this point. Within the core, in both the blue and red-shifted outflow lobes, dP/dR (and probably also ρ_o) has a much shallower gradient.

4.2. Variability in the RNO 15-FIR molecular jet

Curving molecular outflows have been observed in a number of star-forming regions (e.g. Bachiller et al. 1990; Dent, Matthews & Walther 1995; Bence, Richer & Padman 1996; Lefloch, Eislöffel & Lazareff 1996). However, a "wiggling" molecular outflow has, to our knowledge, so far not been reported. Variability in jets is seemingly a common occurance (e.g. López et al 1995; Ray et al. 1996; Heathcote et al. 1996; Eislöffel et al. 1996) so it seems reasonable that jet-driven molecular outflows might also show signs of directional variability.

The high-velocity flow lobes in Fig. 4 hint at regular deviations in the outflow direction from the nominal flow axis. To examine this possibility, we have fit a gaussian profile to the integrated intensity contours in Fig. 4 at 5″ intervals along the RNO 15-FIR outflow axis, each gaussian being perpendicular to the flow axis (note that the major axis of the grid of spectra from which this map was derived is orientated roughly along the outflow axis, at a P.A. $\sim 42°$ E of N). A straight line fit through these points leads to a more precise measure of the orientation of the outflow axis, which we find to be 47.2° E of N.

The centroid of each gaussian fit is plotted in Fig. 7; here, the nominal flow axis is orientated along the x-axis. The deviation of each point from the x-axis we consider as being due to the wiggling of the molecular outflow. The plot in Fig. 7 suggests a sinusoidal distribution. We therefore fit these data with a function of the form $y = \pm A\ sin(2\pi[x - \phi]/\lambda)$, where x is the distance (in arcseconds) along the outflow axis and where the function is *mirror symetric* about $x = \phi$. We have excluded from this least-squares fit data points in the range 0″– 55″, because here the red-shifted lobe of the RNO 15-FIR outflow appears to overlap the red lobe from RNO 15 (see Fig. 4; also, Levreault 1988). To the remaining points we obtain a reasonable fit with an amplitude of A = 1.″4 (0.0024 pc) and a wavelength (projected onto the plain of the sky) of λ = 38.″5 (0.065 pc). We also find that the phase, ϕ = 3″; the true source position may therefore be shifted slightly from the nominal IRAS position used as x = 0 in Fig. 7.

A stellar jet ejected from a source with a time-dependent ejection direction is expected to describe a helical, *point-symmetric* pattern (Raga, Cantó & Biro 1993; Cliffe et al. 1995; Steffen 1996). The amplitude of this pattern should increase from zero because of the opening angle of the helical flow. However, the data in Fig. 7 clearly point to a non-zero amplitude at the source which remains more or less constant along the full length of the flow. We therefore *do not* interpret the observed variation in Fig. 7 in terms of a precessing source. Instead, the

plot and fit are best explained if the outflow source is part of a binary system, both stars being undetected at near-IR wavelengths. The amplitude and wavelength of the fit allow us to very crudely estimate the binary separation (2.″8 = 980 AU) and period ($T \sim [\lambda/sin\theta]/V_{\rm flow}$ = 9050 years; here we assume a flow velocity and inclination angle of $V_{\rm flow}$ = 10 km s^{-1} and $\theta \sim 45^{\circ}$); these values imply a combined mass of roughly 12M$_{\odot}$. Needless to say, VLA observations of the source region would be very useful to confirm this hypothesis.

5. Conclusions

CO J=3-2 observations and a deep, [S II] $\lambda\lambda$6716,6731 image of the bipolar outflow driven by RNO 15-FIR are presented. The close association between the collimated CO outflow and the underlying stellar jet, which is traced by H_2/[S II] line emission features (molecular shocks), suggests that the CO outflow is jet-driven, and that the "prompt" or bow shock entrainment mechanism dominates. The radially decreasing momentum distribution in the CO outflow also adds credence to this interpretation.

Analysis of the CO outflow map also suggests that the flow is "wiggling", with an amplitude of 1.″4 (0.0024 pc) and a wavelength (projected onto the plain of the sky) of 38.″5 (0.065 pc). This motion is best explained if the outflow source is part of a deeply embedded binary star system.

Acknowledgements. We would like to thank Brent Tully for the use of his [SII] filter at the U of H 2.2 m telescope, and the anonymous referee for his/her careful reading of the manuscript and very useful comments. We also thank Iain Coulson and the rest of the JCMT service observing team for their help in completing the CO map. The James Clerk Maxwell Telescope is operated by the Royal Observatories on behalf of the UK Particle Physics and Astronomy Research Council, the Netherlands Organisation for Scientific Research, and the National Research Council of Canada.

References

Bachiller, R., 1996, Ann. Rev. A&A, 34, 111
Bachiller, R., Cernicharo, J., Martín-Pintado, J., Tafalla, M., Lazareff, B., 1990, A&A 231, 174
Bally, J., Devine, D., Hereld, M., Rauscher, B.J. 1993, ApJ 418, L75
Bence, S.J., Richer, J.S. & Padman, R., 1996, MNRAS 279, 866
Bontemps, S., André, P., Terebey, S., Cabrit, S., 1996, A&A 311, 858.
Cabrit, S., 1989, in Low Mass Star Formation and Pre Main Sequence Objects, ed. B. Reipurth (ESO: Garching), p.119
Cabrit, S., Bertout, C., 1990, ApJ 348, 530
Chandler, C.J., Terebey, S., Barsony, M., Moore, T.J.T., Gautier, T.N., 1996, ApJ 471, 308
Chernin, L., Masson, C., 1995a, ApJ 455, 182
Chernin, L., Masson, C., 1995b, ApJ 443, 181
Chernin, L., Masson, C., Gouveia Dal Pino, E. M., Benz, W., 1994, ApJ 426, 204
Cliffe, J.A., Frank, A., Livio, M., Jones, T.W., 1995, ApJ 447, L49.
Cunningham, C.T., Hayward, R.H., Wade, J.D., Davies, S.R., Matheson, D.N., 1992, Int.J.Ir.Millim.Waves, 13, 1827
Davis, C.J., Eislöffel, J., 1995, A&A 300, 851 (Erratum; A&A 305, 694)
Davis, C.J., Mundt, R., Eislöffel, J. 1994, ApJ, 437, L55
Davis, C.J., Ray, T.P., Eislöffel, J., Corcoran, D., 1997, A&A, in press
Dent, W.R.F., Matthews, H.E.M., Walther, D., 1995, MNRAS 277, 193
DeYoung, D.S., 1986, ApJ 307, 62
Eislöffel, J., Smith, M.D., Davis, C.J., Ray, T.P., 1996, AJ 112, 2086
Frerking, M.A., Langer, W.D., 1982, ApJ 256, 523
Fukui, Y., Iwata, T., Mizuno, A., Bally, J., Lane, A., 1993, in Protostars and Planets III, eds... (Univ. Arizona: Tucson), p.
Goldsmith, P.F., Snell, R.L., Hemeon-Heyer, M., Langer, W.D., 1984, ApJ 286, 599
Heathcote, S., Morse, J.A., Hartigan, P., Reipurth, B., Schwartz, R.D., Bally, J., Stone, J.M., 1996, AJ 112, 1141
Herbig., G.H., Jones, B.F., 1983, AJ 88, 1040
Hodapp, K-.W., 1994, ApJS 94, 615
Juan, J., Bachiller, R., Kömpe, C., Martin-Pintado, J., 1993, A&A 270, 432
Kutner, M.L., Ulich, B.L., 1981, ApJ 250, 341
Lada, C.J., Fich, M., 1996, ApJ 459, 638
Ladd, E.F., Hodapp, K-.W., 1996, ApJ ...
Lefloch, B, Eislöffel, J., Lazareff, B., 1996, A&A 313, L17
Levereault, R.M., 1988, ApJS 67, 283
López, R., Raga, A., Riera, A., Anglada, G., Estalella, R., 1995, MNRAS 274, L19.
Masson, C.R., Chernin, L.M., 1992, ApJ 387, L47
Masson, C.R., Chernin, L.M., 1993, ApJ 414, 230
Moriarty-Schieven, G.H., Snell, R.L., 1989, ApJ 338, 952
Mundt, R., Brugel, E.W., Bührke, T., 1987, ApJ 319, 275
Myers, P.C., Fuller, G.A., Goodman, A.A., Benson, P.J., 1991, ApJ 376, 561
Parker, N.D., Padman, R., Scott, P.F., 1991, MNRAS 252, 442
Raga, A.C., Cabrit, S., 1993, A&A 278, 267
Raga, A.C., Cabrit, S., Cantó, J., 1995, MNRAS 273, 422
Raga, A.C., Cantó, J., Biro, S., 1993, MNRAS 260, 163
Ray, T.P., 1996, in Solar and Astrophysical Magnetohydrodynamical Flows, ed. K.C. Tsinganos, (Kluwer:Dordrecht), p.539
Ray, T.P., Mundt, R., Dyson, J.E., Falle, S.A.E.G., Raga, A.C., 1996, ApJ 468, L103
Shu, F.H., Adams, F.C., Lizano, S., ARA&A 25, 23
Stahler, S.W., 1994, ApJ 422, 616
Steffen., W., 1996, Vistas in Astronomy, in press.
Taylor, S.D., Raga, A.C., 1995, A&A 296, 823

This article was processed by the author using Springer-Verlag LaTeX A&A style file *L-AA* version 3.